Network decomposition model to describe the solid and gaseous thermal conductivity in open-porous (nano)materials

Shivangi Aney, Ameya Rege *

Institute of Materials Research, German Aerospace Center (DLR), Linder Höhe, 51147, Cologne, Germany

ARTICLE INFO

ABSTRACT

Understanding the interplay between the heat transport through the solid phase and the porous one may play a vital role in the inverse design of open-porous (nano)materials for thermal superinsulation applications. In this paper, we propose a mechanistic model using the finite element framework to independently describe the thermal transport through the solid phase and the porous one. The proposed model considers heat conduction through the solid and gaseous phases and does not account for convective and radiative effects. To this end, a network decomposition model is proposed wherein the open-porous material is decomposed into a solid network model (SNM) and a pore network model (PNM). An excluded volume concept is further introduced within the PNM, and is driven by the Knudsen diffusion for modelling in the case of nanoporous materials. The model predictions are validated with experimental data and the model is shown to accurately estimate the total thermal conductivity for nanoporous materials where convection and, at room temperature, radiation do not play any significant role.

1. Introduction

To meet the increasing demand for energy-efficient solutions, especially in thermal management, significant emphasis has been placed on the rapid advancement of thermally superinsulating materials. A range of materials can be considered as thermal insulators, namely, glass and mineral wool, cork, expanded polystyrene (EPS) foams, polyurethane foams, to name a few. However, very few materials are characterised as thermal superinsulators, namely, microporous materials and aerogels. These materials have demonstrated thermal conductivities below that of air (around 0.025 W m^{-1} K^{-1} at standard atmospheric pressure and room temperature). Rapid development of thermal insulating materials demands a physics-informed yet computationally fast approach for predicting material properties as well as for reverse engineering of the materials design process.

What drives these materials to perform as thermal insulators is their low thermal conductivity, which is a direct measure of heat flow through the material. One common characteristic of the above-mentioned materials is their open-porous nature. The term open-porous implies the presence of at least two phases in a material, namely a solid phase and an open porous phase. The latter is referred to as the gaseous phase, as it is occupied by a gas, typically air. This phase, being open, is in principle a 3D network of open channels. Thermal conductivity in a material can be characterised by heat transport through three modes, namely, conduction, convection, and radiation. However, since

the open-porous material exhibits two phases, the conduction can occur either through the solid network or through the pore network. By pore network, it is meant that the gas flows through the open-porous interconnected channels. The wider the channels, the easier and higher the amount of flow of gas molecules, while the smaller the channels, the sparser the flow. This in turn affects the molecular collision that results in gaseous conduction. What factor dictates this effect? It is the mean free path of the air, which is close to 70 nm. Thus, materials that exhibit pore sizes larger (hundreds of nm) or significantly larger (μm- or mm-sized) than this value will undergo what we know as continuum flow. The gaseous thermal conductivity is higher for these materials as the probability of gas–gas molecular collisions is very high. On the other hand, materials that exhibit pore sizes much smaller than the mean free path of the air exhibit what we know as Knudsen flow.

Knudsen diffusion refers to the flow that includes only molecule-pore wall collisions (at low pressure, small pores), in contrast to molecular diffusion, which refers to flow involving intermolecular collisions in the gas phase (for high pressures and large pores) [1]. Thus, Knudsen flow occurs when the interactions between the gas molecules and the restrictions in the path (pore walls in case of porous materials) are much higher than the collisions between the individual gas molecules. This necessitates a relative measure of the mean free path of the gaseous medium to the physical length scale of the obstructions (path restrictions) which is defined as the Knudsen number. Knudsen diffusion is

one of the reasons for the very low thermal conductivities in case of nanoporous materials (0.01–0.10 W m^{-1} K^{-1} [2–5]).

The low thermal conductivity of cellular materials and the promise of excellent thermal insulation has led to the development of numerous theoretical, experimental as well as computational approaches to predict the thermal properties of such materials. The modelling of the solid and gaseous thermal conductivity could be categorised based on empirical [5–7], analytical or numerical methods used [8,9]. For example, Fricke and Emmerling [6] surveyed different modelling approaches describing the transport properties and validated them based on the scaling behaviour. This empirical scaling relation has been used to coarsely validate the presented approach. In case of porous materials with complex hierarchical microstructures, the coupling of solid and gaseous thermal conductivity has also been investigated [10–12]. The evaluation of the thermal conductivity due to the solid–gas coupling is beyond the scope of this paper.

Computational approaches have been extensively employed to model the thermal conductivity of porous materials. In such cases, designing the microstructure plays an important role. For example, Finney [13] investigated how fundamental statistical geometry could be used as a powerful tool for tackling important problems in many branches of science and engineering. Several authors developed models accounting for the microstructure to analyse the heat transfer properties through porous medium [14–19]. For example, Bi et al. [16] demonstrated for silica aerogel that simple structures can be used for numerical or analytical studies if the structure is in spatial and periodic symmetry. Dan et al. [17] have used a hollow sphere model independent of empirical parameters, with better agreement with experimental results. Chen et al. [18] modelled the microstructure of aramid nanofiber aerogels using fractal geometry theory. Of particular relevance to this work is the reconstruction of the 3D pore space of cellular materials using Voronoi tessellations. The different forms of Voronoi tessellations prove to be an effective tool to design and predict the structure–property relations in case of open-porous cellular materials [20–25].

In our previous work [26], the porous fibrillar reconstructed microstructure was used for analysing the effect of the pore space on the mechanical properties of open-porous cellular materials. In this work, the same computational method is used to first design the porous structure of a cellular material. A predictive model based on a mechanistic approach is then developed to estimate the solid and gaseous thermal conductivity of the cellular solid. For modelling the Knudsen diffusion in flow, the model ansatz employs the concept of excluded volume, particularly for modelling nanoporous materials. Such an addition can be neglected in case of cellular solids with macropores. Finally, the validation of the presented approach is reported for different porous materials having pore sizes in different length scales.

2. Model definition and methodology

The thermal conductivity is an important parameter to quantify the insulation capabilities as it is a direct measure of heat flow through the material. Due to the two phase nature of the porous materials, the thermal conductivity is accounted for by considering the conduction through the solid skeleton of the material, gaseous conduction through the pores, convection through the gaseous medium as well as radiation. This can be expressed as the following equation,

$$\lambda_t = \lambda_s + \lambda_g + \lambda_c + \lambda_r, \tag{1}$$

where, λ_t is the total thermal conductivity, λ_s, λ_g, λ_c and λ_r are the contributions to the thermal conductivity due to solid conduction, gaseous conduction, convection and radiation, respectively. The principle of superposition allows for the calculation of the individual components of the thermal conductivity (as in Eq. (1)) independently. In this paper, a simplified mechanistic approach is designed which does not account for thermal conductivity due to radiation as it is relatively negligible

at room temperature. Furthermore, since this study is motivated by nanoporous materials, the effect of convection is not considered. Thus, total thermal conductivity is described by the contributions from the remaining two components, namely, the solid and gaseous conduction,

$$\lambda_t = \lambda_s + \lambda_g. \tag{2}$$

The methodology of using resistor networks for modelling thermal conductivity for composite materials has been presented in detail be Yue et al. [19]. This fundamental approach is applied here. The resistor network is a simplistic representation of the microstructure with nodes and resistors between each node pair. The thermal resistance between two nodes (r_{ij}) is a function of the heat transfer coefficient (h), thermal conductivity (λ_{ij}) and cross-section area (A) of the individual resistor ($r_{ij} = \frac{h}{\lambda_{ij}A}$) between the nodes. A temperature difference is applied at the boundaries and the heat flow through the resistor system is calculated. For all nodes, except the boundary nodes, no heat is generated at the nodes, i.e., heat entering the node equals the heat leaving the node. Hence, using energy conservation at each node and solving a system of linear equations for the nodal temperatures, the heat flowing into the resistor network can be calculated. The effective thermal conductivity of the network can then be calculated using the Fourier law of heat conduction,

$$Q = \lambda A \frac{dT}{dx}, \tag{3}$$

where Q is the heat flow through the resistor system which can be simulated, A is the cross-sectional area of the entire network, dT is the applied temperature difference and dx is the size of the simulation domain. With this ansatz, the network model can be easily adapted to the microstructure of open-porous cellular materials.

The porous microstructure of an open-porous cellular material is first computationally designed [25]. In this method, the pore space is reconstructed given an input pore-size distribution which is obtained experimentally. A random close packing of polydisperse spheres (Fig. 1a), with each sphere representing a pore is generated. The sphere pack is the input for the Laguerre–Voronoi tessellations (Fig. 1b). This retains the experimental pore-size information while designing the skeletal network with random-shaped pores. The heat transfer across this material representation occurs through the solid network (Fig. 1c) represented by the Voronoi-cell edges as well as the pore network represented implicitly by the sphere pack. Hence, we can independently derive the effective solid and gaseous thermal conductivity from the solid and pore networks respectively (Eq. (2)). In the case of modelling the effective solid thermal conductivity, material properties of the individual struts (density, thermal conductivity) are defined for the geometrical representation of the solid skeleton. The strut diameters are calculated based on the porosity of the entire representative volume element (RVE) [25]. Since the RVE generated using this computational method is isotropic [20,22,25], a temperature difference can be applied only in one direction to produce a unidirectional heat flux. The effective solid thermal conductivity of the microstructure can be then calculated using Fourier law of heat conduction (Eq. (3)) where the heat flow, cross-sectional area, temperature difference and length of the RVE is known.

While the conduction through the solid network is relatively straightforward, the conduction through the porous space demands further explanation. A 2D slice of the network models is shown in Fig. 1d. The solid lines depict the solid skeleton forming the solid network model (SNM) and the dotted lines depict the pore connectivity or the pore network model (PNM). Thus, comparing the network models with resistor networks, the nodes are the vertices (v_i in Fig. 1d) of the Voronoi geometry in SNM and the pore/sphere centres (c_i in Fig. 1d) in PNM. The resistors in the SNM are the edges of the Voronoi cells while in case of the PNM, these are the connections between the cell centres.
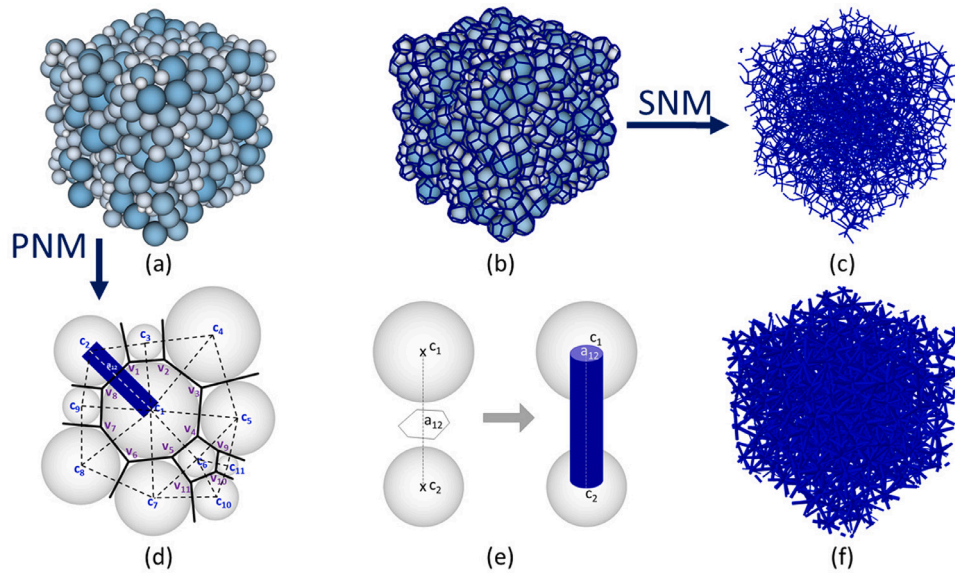
Fig. 1. Network models for predicting the effective thermal conductivity: (a) Pore connectivity represented by the sphere pack, (b) microstructural representation with pores (spheres) and fibrillar pore walls (edges), (c) representative volume element (RVE) of the solid network, (d) pore connectivity in 2D (represented by dotted lines), (e) approximation of the pore cross-sectional area for the PNM, (f) RVE of the pore network.
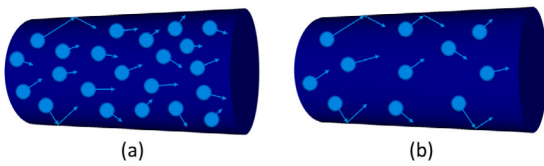

Fig. 2. (a) Bulk diffusion, (b) Knudsen diffusion.

The pore network (as shown by the dotted lines in Fig. 1d) is representative of the pore connectivity. In mathematical terms, the pore network is the dual (i.e., the Delaunay tessellations) of the solid network represented by the Voronoi tessellation. The PNM essentially captures this pore connectivity of the microstructure and uses it to model the effective gaseous thermal conductivity. The modelling of the effective gaseous thermal conductivity is slightly challenging although the ansatz remains the same. It is assumed that the heat transfer occurring between the two pores takes place only through the Voronoi face between them (see Fig. 1e). Thus, the smaller the adjacent pore, the smaller is the cross-sectional area and correspondingly, the heat flow to the pore. This heat transfer can be approximated by a resistor channel (see Fig. 1e) between the pore centres. The length of this resistor is the centre distance, its thermal conductivity is the thermal conductivity of the medium and the cross-sectional area of the resistor channel is a function of the area of the Voronoi face between the two pores (a_{12}). The exact area of these channels depends on the porosity and the size of the adjacent pore (see Fig. 1d and e). This cross-sectional area is calculated considering the gas fraction of the RVE, which is the total volume that can be occupied by the gaseous medium. It can be expressed in terms of the solid fraction as $\phi_g = 1 - \phi_s$. The actual RVE as a network of pore channels of different cross-sectional areas is shown in Fig. 1f.

In the case of continuum flow, the cross-sectional area of the resistor can be approximated by the area of the Voronoi face between the end nodes (sphere centres) of the resistor. However, for nanoporous materials where Knudsen diffusion is predominant, the cross-sectional area of the resistor channel is assumed as only a fraction of the area of the corresponding Voronoi face. To understand this assumption and model the heat flow through the resistor channels of the PNM, we evaluate the flow through these channels (refer Fig. 2). Firstly, the Knudsen number is defined as,

$$K_n = \frac{l}{d_c}, \tag{4}$$

where l is the mean free path of the gaseous medium and d_c is the diameter of the channel. For very low Knudsen numbers, continuum flow is observed while for very high Knudsen numbers we get molecular flow. Secondly, to include the effect of Knudsen diffusion, a fraction of the channel volume is excluded to account for the difference in the volume occupied by molecules undergoing molecular collision through the channel in comparison to the case of continuum flow. In the case of high Knudsen numbers, (molecular flow) the probability of such molecular collisions occurring in a pore is lesser as compared to that in continuum flow. This is because the interactions between the molecules and the pore walls will be much higher than the interactions between the molecules. Hence, the excluded volume will be higher for larger Knudsen numbers. The excluded volume can thus be seen as a factor affecting the modelling of thermal conductivity in this porous space and is shown to be calculated in direct correlation with the Knudsen number.

The finite element model was principally similar for the SNM and PNM, with minor modifications for the PNM to include the excluded volume parameter. The resistors or cylindrical channels (Voronoi edges in the case of SNM and pore channels in the case of PNM) were modelled as 1D line elements with temperature degree of freedom. The thermal properties of the solid material and air were used as inputs to the finite element model based on SNM and PNM, respectively. The temperature difference was effectively applied by maintaining the boundary nodes of the RVEs at 300 K and 350 K. The heat flow through the RVEs due to this temperature difference was subsequently simulated under steady state conditions. In the absence of external thermal loads, the surfaces of the cylindrical channels constituting the SNM and PNM can be assumed as isolated in the finite element model. Thus, the heat flow simulated using the finite element model corresponds exclusively to the heat transfer through the SNM and PNM channels. Due to this nature of the finite element simulation, the cross-sectional area of the channels represented by these line elements have a critical influence on the prediction of the thermal conductivity. The methodology of determining the cross-sectional areas was described earlier in this section. The sensitivity of the model to the excluded volume along with other model parameters has been analysed and reported in the following section.
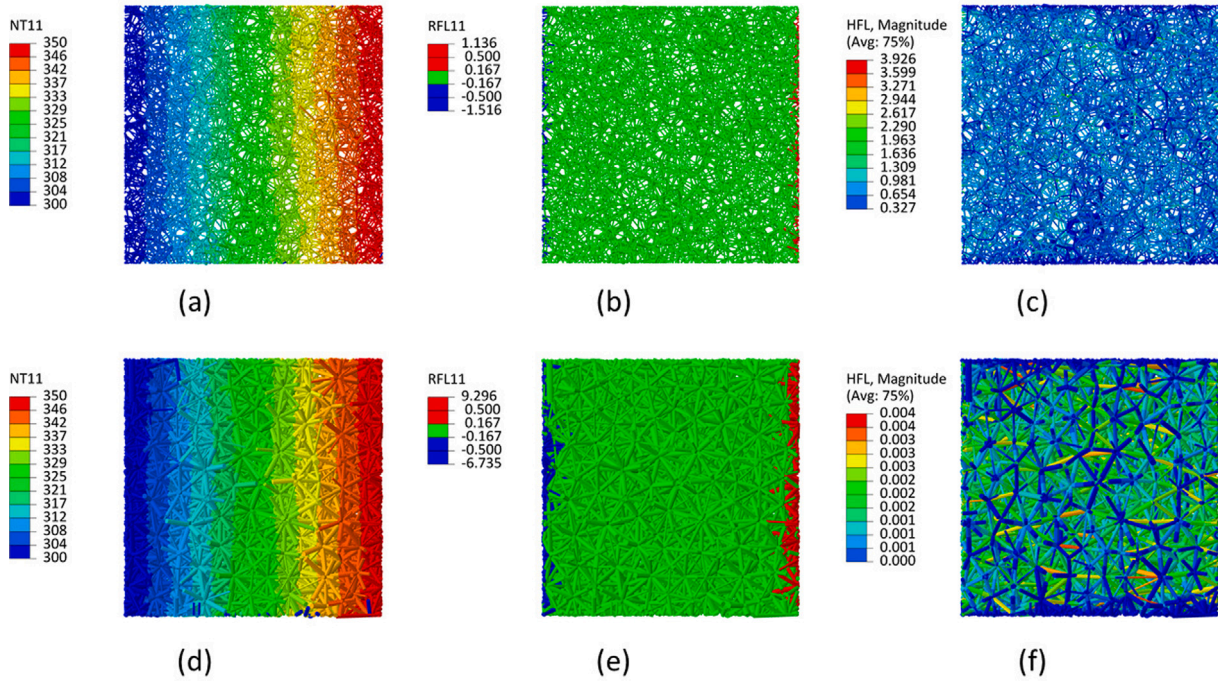
Fig. 3. Visualisation of finite element results: (a) Temperature distribution in SNM, (b) reaction fluxes for the temperature difference in SNM, (c) heat flux per unit area for the temperature difference in SNM, (d) temperature distribution in PNM, (e) reaction fluxes for the temperature difference in PNM, (f) heat flux per unit area for the temperature difference in PNM.

3. Results

This section presents the first results of the model and a parameter sensitivity analysis followed by the validation of the model for different materials with different length scales. To obtain the first results, the porous microstructure was reconstructed computationally with an input pore-size distribution. A normal distribution function with a mean pore size of 50 nm and the standard deviation of 20 nm was used. The porosity of the microstructure was maintained at 95%. These values of the mean pore-size and the porosity are representative of commonly known nanoporous materials. The SNM and PNM were developed using the methodology detailed in Section 2. The RVE had a size of 450 nm and was simulated by applying a temperature difference of 50 K across the length of the domain in the x direction using Abaqus. In this study, air has been used as the gaseous medium and is modelled using the characteristics at standard atmospheric pressure.

The finite element visualisations for the SNM and PNM can be observed in Fig. 3. The variations in the nodal temperatures are illustrated for the solid and gaseous networks in Fig. 3a and d. While simulating the heat transfer using Abaqus, the output variables were the heat fluxes. The heat flow can be calculated from the fluxes by simulating for steady state heat transfer. The visualisations shown in Fig. 3 thus correspond to the heat fluxes at steady state. The RFL11 represents the reaction flux due to the applied boundary conditions in the x direction. The reaction fluxes are obtained only at the boundaries of the RVE. Although the reaction fluxes can be used to calculate the heat flow through the network, this calculation is more streamlined by using the HFL, which is the heat flux per unit area. Owing to computational convenience, in this work the HFL was used to calculate the thermal conductivity from the Fourier's law of heat conduction as follows:

$$\lambda = \frac{\sum\limits_{i=0}^{n} Q_i \cdot dx}{A \cdot dT} \tag{5}$$

where Q_i is the heat flowing through the ith node on the RVE boundary, n is the total number of nodes on the RVE boundary, dx is the length of the RVE, in this case 450 nm, dT is the applied temperature difference

Table 1
Gaseous thermal conductivity values (in W m^{-1} K^{-1}) for different excluded volumes.

Ev	0.02	0.10	0.20	0.40	0.60
Kn_{eff}	1.43	1.55	1.75	2.33	3.5
λ_g	0.018	0.015	0.013	0.009	0.006

of 50 K and A is the cross-sectional area of the RVE. The heat flow (Q_i) for the individual node is calculated from the HFL flux per unit area at steady state (Q_{hfl}) as follows:

$$Q_i = Q_{hfl} \cdot Ac_i \cdot (1 - Ev_i) \tag{6}$$

where Ac_i is the cross-sectional area of the corresponding channel and Ev_i is the excluded volume (Ev_i is only applicable to PNM). It is to be noted that even though the volume is excluded, this should not change the length of the individual elements as a change in length would result in a disconnected network. Therefore, the excluded volume is totally reflected by the change in the cross-sectional area. For the above-defined input values the solid thermal conductivity of 0.015 W m^{-1} K^{-1} was calculated using the SNM.

The gaseous thermal conductivity is influenced by the excluded volume (Eq. (6)). The dependence of the gaseous thermal conductivity on the excluded volume (Ev) and the corresponding effective Knudsen number (Kn_{eff}) is tabularised in Table 1. As the excluded volume increases, the channel cross-sectional area decreases, thereby decreasing the heat flow through the network. Simultaneously, as the channel cross-sectional area decreases, the effective Knudsen number increases.

3.1. Effect of excluded volume

The motivation of using excluded volume to map the predicted thermal conductivity of nanoporous materials is derived from Knudsen diffusion. Several theoretical models predicting the gaseous thermal conductivity are formulated on the basis of the Knudsen number [27, 28]. Hence, it is important to evaluate the trends between the excluded volume, the Knudsen number and the predicted gaseous thermal conductivity (refer Fig. 4).
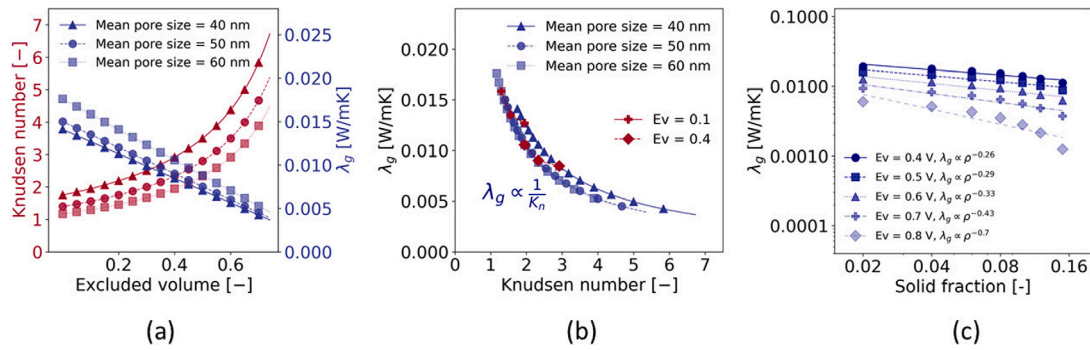
Fig. 4. Correlating the excluded volume with Knudsen number: (a) Effect of excluded volume on Knudsen number and predicted gaseous thermal conductivity, (b) verification of the trend between gaseous thermal conductivity and Knudsen number, (c) effect of excluded volume on scaling exponents of empirical power law relation.
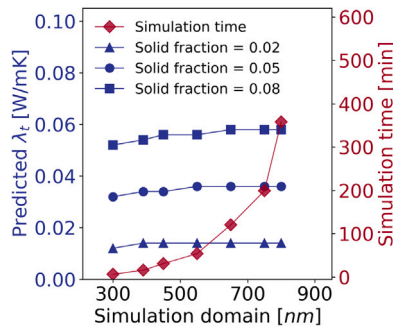

Fig. 5. Effect of the RVE size on thermal conductivity and comparison to the consequent computing time.

Table 2

Effect of direction of applied temperature on λ_s (expressed in W m^{-1} K^{-1}).

Solid fraction	0.02	0.08	0.16
x	0.004	0.014	0.029
y	0.004	0.014	0.028
z	0.004	0.015	0.030

Table 3

Effect of direction of applied temperature on λ_g (expressed in W m^{-1} K^{-1}).

Solid fraction	0.02	0.08	0.16
x	0.007	0.006	0.005
y	0.007	0.006	0.004
z	0.007	0.006	0.005

In this work, three random microstructures were generated with different pore-size distributions characterised by a normal distribution function. The mean pore sizes of 40 nm, 50 nm and 60 nm were considered and the standard deviation was kept constant at 8 nm. The pore network was then simulated by excluding a portion of the channel volume. This excluded volume was quantified as a fraction of the total simulation volume. Thus, an excluded volume of 0.2 implies that 20% of the total simulation volume is excluded from the channels representing the pore network. As the excluded volume increases, the diameter of the PNM channels decreases thereby increasing the corresponding effective Knudsen number (Eq. (4)). This decrease in the channel diameters implies that less heat flows through the channels considering Fourier's law of heat conduction (Eq. (3)). Therefore, the gaseous thermal conductivity decreases with excluding more volume. These results are shown in Fig. 4a. It is also observed that as the mean pore size increases, the Knudsen number decreases and the gaseous thermal conductivity increases. This trend is depicted in Fig. 4b and is often found in theoretical models which predict the gaseous thermal conductivity based on the Knudsen number. This further validates our model.

While, the trends captured in the plots in Fig. 4a and b show the expected correlations from the literature between the excluded volume, Knudsen number and gaseous thermal conductivity, this does not answer how the value of the excluded volume is determined. To estimate the exact value or at least a range of the values of the volume to be excluded, the influence of the excluded volume on the scaling exponent is evaluated first. Open porous materials often exhibit power scaling laws for the mechanical, thermal and acoustic properties with respect to their densities [29–31]. In this case, the exponent (α) with which the effective gaseous thermal conductivity scales with the solid fraction ($\lambda_g \propto \rho^\alpha$) is studied. Since the gaseous thermal conductivity for open-porous nanomaterials typically decreases with an increase in the solid fraction, the scaling exponents obtained are negative, e.g., refer to the article by Fricke et al. [6].

The evaluation of the effect of the excluded volume on the scaling exponent provides information on the range of the volume that can be excluded. This is demonstrated by the results in Fig. 4c. The correlations of the excluded volume with the Knudsen number and the corresponding gaseous thermal conductivity, as exemplarily tabularised in Table 1 along with the graphical representation in Fig. 4c, provide important insights regarding the use of the excluded volume.

3.2. Effect of computational parameters

The computational parameters should not ideally influence the model predictions. To this end, in this section, the sensitivity of the model to the computational factors such as RVE size and the directional dependency of the applied temperature gradient, particularly for isotropic materials, is evaluated. First, the negligible effect of the directional dependency is verified. The solid and gaseous thermal conductivities are simulated for three different solid fractions. An excluded volume of 50% was used for the PNM.

The resulting solid and gaseous thermal conductivities are listed in the Tables 2 and 3 respectively confirming that the computationally reconstructed microstructure is isotropic.

The size of the simulation domain is also an important factor that affects the accuracy of the predictions. The domain size is often a trade-off between accuracy and computational efficiency. Normally, for microstructure simulations, the RVE size is chosen such that it can effectively capture the variations in the pore sizes and remains insensitive to the simulated properties. In this work, the RVE size was varied from 300 nm to 800 nm for the same pore-size distribution and the heat flow through the network was simulated for three different solid fractions. The resulting total thermal conductivity and the required simulation time is shown in Fig. 5. The error in the predicted thermal conductivity changes only marginally for larger RVE sizes, particularly beyond 400–450 nm. In contrast the simulation time increases exponentially from 7 min for an RVE size of 300 nm to approximately 6 h for a RVE size of 800 nm. The simulation time plotted in Fig. 5 consists of the time
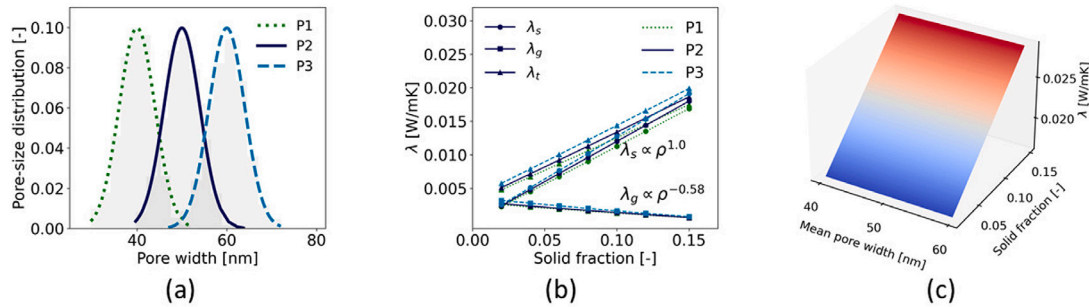
Fig. 6. (a) The different pore-size distributions considered, based on the variation of the mean pore sizes, (b) the influence of the mean pore size on the solid, gaseous, and effective total thermal conductivity, (c) surface plot illustrating this change in the effective total thermal conductivity.

Table 4
Effective thermal conductivity values (expressed in W m^{-1} K^{-1}) predicted for different materials.

Material	Mean pore size	λ_t experiment	λ_t predicted
Aluminium foam [32]	2.3 mm	4.6	3.528
Polyurethane foam [33]	3.1 mm	0.044	0.034
Polyetherimide nanofoam [34]	86 nm	0.015	0.014
Biopolymer aerogel [3]	50 nm	0.028	0.023

required for structure generation and the simulation in Abaqus. Since the post-processing of the results is automated, the post-processing time is not considered. The exponential increase in the simulation time is mainly attributed to the exponential increase in the complexity of the microstructure as a result of increasing the RVE size. For example, as the simulation domain size increases from 300 nm to 800 nm, the number of pores contained in it increases from 500 to 10 000. The total nodes in the network increase from 3865 and 1751 to 65 672 and 19 636 for SNM and PNM, respectively. Similarly, the total elements in the network increase from 8724 and 3542 to 139 201 and 70 329 for SNM and PNM, respectively. Hence, the size of the RVEs used in this study are in the range of 400–450 nm given that sizes beyond these did not yield in significantly improved results.

3.3. Effect of the pore-size distribution

The pore-size distribution plays an important role while predicting the material properties of polydisperse open-porous materials [26]. The computational geometry used in this model is reconstructed using an input pore-size distribution. Typically, a normal distribution function can be used to describe the pore-size distribution. While the distribution in typical nanoporous materials is non-Gaussian in nature, for simplicity, in this work, the variation of the predicted solid and gaseous thermal conductivities due to the change in the mean pore size and the standard deviation of the pore-size distribution is analysed using a Gaussian distribution of the pore sizes. Two sets of examples were chosen where the mean pore size and the standard deviation in the pore sizes was varied. First, the mean pore size was varied from 40 nm to 60 nm as illustrated in Fig. 6a. The resulting thermal conductivities are plotted in Fig. 6b for estimating the scaling exponent. The solid thermal conductivity scales with an exponent of 1.0 while the gaseous thermal conductivity scales with an exponent of −0.58. For all other parameters kept constant, the mean pore size does not have a very significant influence on the thermal conductivity especially for smaller solid fractions. Although the scaling trend is observed to be similar for all three pore-size distributions, the variations in the solid thermal conductivity are larger for larger solid fractions. In case of the gaseous thermal conductivities, the deviations with changing pore sizes are marginal when the mean pore size is increased from 40 nm to 60 nm. However, this may not be the case when the mean pore size is changed significantly (for example from 40 nm to 150 nm, which changes the

Knudsen number from 1.75 to 0.47). It is evident from the results that although the mean pore size affects the predicted thermal conductivity, it has no influence on the scaling exponent at all. Similar results were obtained by varying the standard deviation for constant mean pore sizes.

For the simulated cases, the total thermal conductivity varies from 0.006 W m^{-1} K^{-1} to 0.020 W m^{-1} K^{-1} as the porosity is changed from 98% to 85% in both sets of examples. This is due to the pore structure and properties selected for the analysis. Thermal conductivities around and below 0.020 W m^{-1} K^{-1} are known for aerogels and other superinsulation materials [2–5]. However, the applicability of the model remains for materials with lower porosities, those well below 85%. Furthermore, in the case of the scaling exponents, the ratio of the elastic (E vs. ρ^m) and thermal (λ_s vs. ρ^t) scaling exponents (m/t) was found to be 2.0, which lies in correlation with the available literature [29]. Thus, with the thermal conductivity values in the expected range and the universal scaling law empirically verified, we can safely conclude that the novel approach presented in this paper can be used to model the effective thermal conductivity for nanoporous materials. One may even import material geometries from computer tomography scans or other computational reconstructions to exploit this approach of SNM and PNM for diverse use cases, and the network decomposition is not restricted to the proposed modelling strategy of Voronoi tessellations. To further validate the application of this method, the effective solid and gaseous thermal conductivities were simulated for a wide range of materials. These results are documented in the following section.

3.4. Model validation

The predicted thermal conductivity depends on various factors such as the skeletal thermal conductivity, the skeletal density as well as the actual pore-size distribution. Hence, to check the accuracy and applicability of this model, it is validated for different materials with different length scales. These include aluminium foam and polyurethane foam with mean pore sizes in the millimeter range as well as polyetherimide nanofoam and biopolymer aerogel with pore sizes in the nanometer range. The microstructural details of the materials were found in the literature and the thermal conductivities were calculated using the SNM and PNM. The predicted thermal conductivity and its components are noted in Table 4. It is observed that since the network models do not account for the thermal conductivity due to the convection, the predicted total thermal conductivity is underestimated in case of conventional foams with cell sizes in millimeter range (refer Fig. 7). Also for such large pore sizes, the averaging of the cross-section area of the pore channels will underpredict the thermal conductivity. Metal foams are known to show high Nusselt number, thus quantifying the ratio between the (total heat transfer) to conductive heat transfer [35]. Several studies have experimentally explored the contribution of convection to heat transfer in aluminium foams [36,37]. Soloveva et al. [33] studied the increasing effect of convection in PU foams with pore sizes and temperature. As a consequence, for such larger pored-structures,
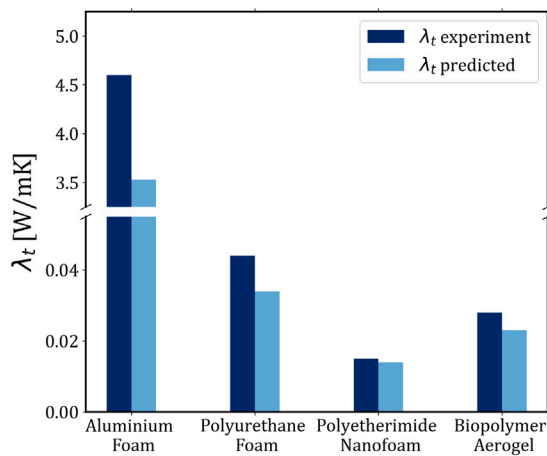
Fig. 7. Model validation for the effective thermal conductivity for different materials. The aluminium foam and polyurethane foam have pore sizes in mm, while the polyetherimide nanofoam and biopolymer aerogel have pore sizes in nm. Thus, the model predictions are more accurate for the latter two than the former two, in which case convection may also play an important role.

convection may certainly play an important role. However, the network model can still be used to predict the interplay between the effective solid and gaseous thermal conductivity components even for such conventional foams. In the case of nanoporous materials at room temperature, the estimation of the total thermal conductivity using the network models is very close to the actual value. Minor deviations may always exist, e.g., in the case of biopolymer aerogels, there is a small proportion of large pores (>200 nm) which are not accounted for by the experimental setup to describe the pore-size distributions. Thus, neglecting these tiny proportion of large pores may result in under-predicting the thermal conductivity, as can be observed in the presented results.

The presented approach is a physically motivated yet a mechanistic approach that can describe λ_s and λ_g for any open-porous material given the information of their microstructure is known. The model is accurate for predicting λ for nanoporous materials, however, for macroporous ones, the model may still be found useful.

4. Conclusions

The paper reports a novel approach to model thermal conductivity due to solid and gaseous conduction in open-porous materials using finite element calculations. The material network is decomposed into a solid network model (SNM) and a pore network model (PNM). For both models, Fourier's law of heat conduction is applied to calculate the heat transport through the skeletal backbone of the material as well as through the channels of pores within the network. For the case of nanoporous materials, an excluded volume concept is introduced within the PNM which is calculated based on the Knudsen number. The model has been validated against aluminium foams and polyurethane foams, which exhibit pore sizes in mm ranges, and polyetherimide nanofoams and biopolymer aerogels, which exhibit pore sizes in nm. For the former two cases, while the trends are captured, quantitative validation could not be achieved given the higher Nusselt numbers exhibiting a higher contribution from convection. Another reason is the averaging of the cross-section area of the pore network channels which underpredicts the thermal conductivity through the porous phase in cases of continuum flow. On the other hand, for the latter two cases, very good agreement could be obtained. This is because convective effects do not play a role in the lower nanometer range. Thus, the model successfully demonstrates predictive capabilities for describing the effective thermal conductivity in open-porous (nano)materials while considering the contributions from solid and gaseous heat conduction.

CRediT authorship contribution statement

Shivangi Aney: Writing – original draft, Visualization, Validation, Methodology, Investigation, Formal analysis. **Ameya Rege:** Writing – review & editing, Supervision, Methodology, Formal analysis, Conceptualization.

Declaration of competing interest

The authors declare that they have no known competing financial interests or personal relationships that could have appeared to influence the work reported in this paper.

Data availability

Data will be made available on request.

References

[1] T.J. Mays, B. Mcenaney, B. Kelly, Gaseous diffusion and pore structure in nuclear graphites, 1996.

[2] D. Illera, J. Mesa, H. Gomez, H. Maury, Cellulose aerogels for thermal insulation in buildings: trends and challenges, Coatings 8 (10) (2018) 345.

[3] S. Zhao, W.J. Malfait, N. Guerrero-Alburquerque, M.M. Koebel, G. Nyström, Biopolymer aerogels and foams: Chemistry, properties, and applications, Angew. Chem. Int. Ed. 57 (26) (2018) 7580–7608.

[4] B. Merillas, J.P. Vareda, J. Martín-de León, M.Á. Rodríguez-Pérez, L. Durães, Thermal conductivity of nanoporous materials: where is the limit? Polymers 14 (13) (2022) 2556.

[5] X. Lu, O. Nilsson, J. Fricke, R.W. Pekala, Thermal and electrical conductivity of monolithic carbon aerogels, J. Appl. Phys. 73 (2) (1993) 581–584.

[6] J. Fricke, X. Lu, P. Wang, D. Büttner, U. Heinemann, Optimization of monolithic silica aerogel insulants, Int. J. Heat Mass Transfer 35 (9) (1992) 2305–2309.

[7] I. Sánchez-Calderón, V. Bernardo, J. Martín-de León, M.Á. Rodríguez-Pérez, Thermal conductivity of low-density micro-and nanocellular poly (methyl-methacrylate)(PMMA): Experimental and modeling, Mater. Des. 221 (2022) 110938.

[8] J.-J. Zhao, Y.-Y. Duan, X.-D. Wang, B.-X. Wang, Effects of solid–gas coupling and pore and particle microstructures on the effective gaseous thermal conductivity in aerogels, J. Nanoparticle Rese. 14 (2012) 1–15.

[9] J.-S. Kwon, C.H. Jang, H. Jung, T.-H. Song, Effective thermal conductivity of various filling materials for vacuum insulation panels, Int. J. Heat Mass Transfer 52 (23–24) (2009) 5525–5532.

[10] J.-J. Zhao, Y.-Y. Duan, X.-D. Wang, B.-X. Wang, A 3-D numerical heat transfer model for silica aerogels based on the porous secondary nanoparticle aggregate structure, J. Non-Cryst. Solids 358 (10) (2012) 1287–1297.

[11] S.S. Shrestha, J. Tiwari, A. Rai, D.E. Hun, D. Howard, A.O. Desjarlais, M. Francoeur, T. Feng, Solid and gas thermal conductivity models improvement and validation in various porous insulation materials, Int. J. Therm. Sci. 187 (2023) 108164.

[12] J. Liu, P. Buahom, C. Lu, H. Yu, C.B. Park, Microscopic revelation of the solid–gas coupling and knudsen effect on the thermal conductivity of silica aerogel with inter-connected pores, Sci. Rep. 12 (1) (2022) 21034.

[13] J. Finney, Random packings and the structure of simple liquids. I. The geometry of random close packing, Proc. R. Soc. A 319 (1539) (1970) 479–493.

[14] D. Baillis, R. Coquard, L. Moura, Heat transfer in cellulose-based aerogels: Analytical modelling and measurements, Energy 84 (2015) 732–744.

[15] T. Tillotson, J. Fricke, Aerogels: Production, characterization and application, Thin Solid Film 297 (1997) 212–223.

[16] C. Bi, G. Tang, Z. Hu, Heat conduction modeling in 3-D ordered structures for prediction of aerogel thermal conductivity, Int. J. Heat Mass Transfer 73 (2014) 103–109.

[17] D. Dan, H. Zhang, W.-Q. Tao, Effective structure of aerogels and decomposed contributions of its thermal conductivity, Appl. Therm. Eng. 72 (1) (2014) 2–9.

[18] X. Chen, Y. Hu, X. Zhuang, X. Wang, Study on pore size distribution and thermal conductivity of aramid nanofiber aerogels based on fractal theory, J. Appl. Phys. 130 (22) (2021) 225104.

[19] C. Yue, Y. Zhang, Z. Hu, J. Liu, Z. Cheng, Modeling of the effective thermal conductivity of composite materials with FEM based on resistor networks approach, Microsyst. Technol. 16 (2010) 633–639.

[20] J. Alsayednoor, P. Harrison, Evaluating the performance of microstructure generation algorithms for 2-d foam-like representative volume elements, Mech. Mater. 98 (2016) 44–58.

[21] G. Cheng, A. Yu, P. Zulli, Evaluation of effective thermal conductivity from the structure of a packed bed, Chem. Eng. Sci. 54 (19) (1999) 4199–4209.

[22] M. Zhang, J. Shang, S. Guo, B. Hur, X. Yue, Numerical investigation of effective thermal conductivity of strut-based cellular structures designed by spatial voronoi tessellation, Materials 14 (1) (2020) 138.

[23] H. Wang, B. Liu, Y.-X. Kang, Q.-H. Qin, Analysing effective thermal conductivity of 2D closed-cell foam based on shrunk voronoi tessellations, Arch. Mech. 69 (6) (2017) 451–470.

[24] L. Bogunia, S. Buchen, K. Weinberg, Microstructure characterization and stochastic modeling of open-cell foam based on μCT-image analysis, GAMM-Mitt. 45 (3–4) (2022) e202200018.

[25] R. Chandrasekaran, M. Hillgärtner, K. Ganesan, B. Milow, M. Itskov, A. Rege, Computational design of biopolymer aerogels and predictive modelling of their nanostructure and mechanical behaviour, Sci. Rep. 11 (1) (2021) 1–10.

[26] S. Aney, A. Rege, The effect of pore sizes on the elastic behaviour of open-porous cellular materials, Math. Mech. Solids 28 (7) (2023) 1624–1634.

[27] Z. Fu, J. Corker, T. Papathanasiou, Y. Wang, Y. Zhou, O.A. Madyan, F. Liao, M. Fan, Critical review on the thermal conductivity modelling of silica aerogel composites, J. Build. Eng. 57 (2022) 104814.

[28] A. Rege, B. Milow, Theoretical modeling of the thermal and mechanical structure-property relationships in aerogels, Aerogels Energy Sav. Storage (2024) 473–496.

[29] L. Weigold, G. Reichenauer, Correlation between mechanical stiffness and thermal transport along the solid framework of a uniaxially compressed polyurea aerogel, J. Non-Cryst. Solids 406 (2014) 73–78.

[30] T. Budtova, T. Lokki, S. Malakooti, A. Rege, H. Lu, B. Milow, J. Vapaavuori, S.L. Vivod, Acoustic properties of aerogels: Current status and prospects, Adv. Eng. Mater. 25 (2023).

[31] S. Aney, P. Pandit, L. Ratke, B. Milow, A. Rege, On the origin of power-scaling exponents in silica aerogels, J. Sol-Gel Sci. Technol. (2023).

[32] Y. Amani, A. Takahashi, P. Chantrenne, S. Maruyama, S. Dancette, E. Maire, Thermal conductivity of highly porous metal foams: Experimental and image based finite element analysis, Int. J. Heat Mass Transfer 122 (2018) 1–10.

[33] O.V. Soloveva, S.A. Solovev, Y.V. Vankov, R.Z. Shakurova, Experimental studies of the effective thermal conductivity of polyurethane foams with different morphologies, Processes 10 (11) (2022) 2257.

[34] S.S. Sundarram, W. Li, On thermal conductivity of micro-and nanocellular polymer foams, Polym. Eng. Sci. 53 (9) (2013) 1901–1909.

[35] K. Yogi, S. Krishnan, S. Prabhu, Influence of metal foam thickness on the conduction and convective heat transfer for a flat plate with metal foam impinged by a rectangular slot jet, Int. J. Therm. Sci. 179 (2022) 107665.

[36] P.M. Kamath, C. Balaji, S. Venkateshan, Convection heat transfer from aluminium and copper foams in a vertical channel–an experimental study, Int. J. Therm. Sci. 64 (2013) 1–10.

[37] A. Hamadouche, R. Nebbali, H. Benahmed, A. Kouidri, A. Bousri, Experimental investigation of convective heat transfer in an open-cell aluminum foams, Exp. Therm Fluid Sci. 71 (2016) 86–94.